

JPEG Compression-Resistant Low-Mid Adversarial Perturbation against Unauthorized Face Recognition System

Jiaming Zhang¹, Qi Yi¹ and Jitao Sang¹

¹Beijing Jiaotong University

jiamingzhang@bjtu.edu.cn, 21125273@bjtu.edu.cn, jtsang@bjtu.edu.cn

Abstract

It has been observed that the unauthorized use of face recognition system raises privacy problems. Using adversarial perturbations provides one possible solution to address this issue. A critical issue to exploit adversarial perturbation against unauthorized face recognition system is that: The images uploaded to the web need to be processed by JPEG compression, which weakens the effectiveness of adversarial perturbation. Existing JPEG compression-resistant methods fails to achieve a balance among compression resistance, transferability, and attack effectiveness. To this end, we propose a more natural solution called *low frequency adversarial perturbation* (LFAP). Instead of restricting the adversarial perturbations, we turn to regularize the source model to employing more low-frequency features by adversarial training. Moreover, to better influence model in different frequency components, we proposed the refined *low-mid frequency adversarial perturbation* (LMFAP) considering the mid frequency components as the productive complement. We designed a variety of settings in this study to simulate the real-world application scenario, including cross backbones, supervisory heads, training datasets and testing datasets. Quantitative and qualitative experimental results validate the effectiveness of proposed solutions.

1 Introduction

In recent years, face recognition system (FRS) has been widely adopted in applications like security unlock, digital ticket and even face payment. However, the privacy problems caused by the unauthorized use of FRS has never been stopped. *E.g.*, a company called Clearview was disclosed to crawl face images from Facebook, YouTube and other online social websites, and provide API to search for someone's face data on the web. There are many studies dedicated to protecting the privacy of users' faces. Some of these works proposed adversarial example solution to protect the online shared face images from the unauthorized FRS [Zhang *et al.*, 2020], where the adversarial example is imperceptible to human but can fool the unauthorized FRS.

While these works aim to improve the attack success rates of adversarial examples. But images uploaded to the web

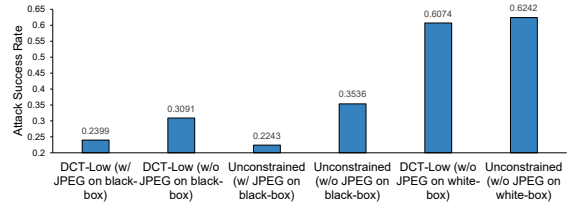


Figure 1: The attack success rates corresponding to different types of adversarial perturbations. DCT-Low is the adversarial perturbations removed high frequency components, Unconstrained is the original adversarial perturbations. The quality factor of JPEG compression is set to be 50.

need to be processed by image compression, *i.e.*, JPEG compression, the most commonly used method on the Internet. It is a defense that removes the high frequency components to weaken the adversarial perturbation. There are several solutions to resist JPEG compression: (1) some works are based on the idea of BPDA [Athalye *et al.*, 2018], replacing non-differentiable JPEG with differentiable mathematical functions [Shin and Song, 2018], or training a generative network to simulate JPEG [Wang *et al.*, 2020c]; (2) The other works try to restrict the adversarial perturbation to the low frequency band of the image assuming that JPEG eliminates noise in the high frequency band [Zhou *et al.*, 2018; Yash *et al.*, 2019]. Low frequency adversarial perturbation is more practical because it does not require the consideration of the specific parameters of JPEG as the former and has proven to exhibit more transferability across networks.

However, it is not an optimal solution if the source model¹ utilizes components not only in the low frequency band, but also enforces the resulting adversarial perturbations to be only in the low frequency band. As shown in Figure 1, (1) Unconstrained (w/ JPEG on black-box) performs worse than Unconstrained (w/o JPEG on black-box). The decreased rate proves that JPEG compression diminish the effectiveness of adversarial perturbations; (2) DCT-Low (w/ JPEG on black-box) performs better than Unconstrained (w/ JPEG on black-box). This indicates that this low frequency adversarial perturbation has more capability to resist JPEG compression than

¹The source model refers to the model that generates the adversarial examples.

the original perturbation; (3) But DCT-Low (w/o JPEG on black-box) performs worse than Unconstrained (w/o JPEG on black-box). This illustrates that restricting the adversarial perturbation weaken the performance of adversarial perturbation in some cases. The details are described in Section 5.2. Therefore, a more natural way is to design the effective low frequency perturbation from redesigning the source model instead of restricting the adversarial perturbation.

To achieve this, we present a new type of *low frequency adversarial perturbation* (LFAP) via robust training process. This allows the source model to utilize information mainly in the low frequency band in the expectation that the adversarial perturbation generated on the robust source model contains more low frequency component. Moreover, by analyzing the impact of full frequency domain components, we find that the mid frequency components still make a non-trivial contribution. So we integrate two models using relative low and mid frequency components to generate the *low-mid frequency adversarial perturbation* (LMFAP).

Since our methods focus on the source model, they can be incorporated with different attack algorithms. In addition, to solidly demonstrate the effectiveness of our methods in practical applications, we designed a variety of black-box settings in this study, including cross backbones, supervisory heads, training datasets and testing datasets of FRS, which is unprecedented in current researches. The contributions of this paper can be summarized as follows:

- We presented a novel method to generate JPEG compression-resistant low-mid adversarial perturbation. This adversarial perturbation can protect the privacy of face images uploaded to social platforms from the authorized FRS.
- We proposed the LFAP via robust training process. We developed ensemble adversarial attacks to propose the refined LMFAP.
- We showed our methods (both LFAP and LMFAP) can be incorporated with existing black-box attack algorithms and significantly improve their performance on a variety of black-box settings.

2 Background and Related Work

2.1 Preliminaries

A complete FRS consists of two modules: the backbone network f used to extract features, such as ResNet50, and the supervisory head h used during training, such as ArcFace. Given an original image \mathbf{x} , f outputs an l -dimension embedding $f(\mathbf{x})$. In the training phase, the FRS is optimized by an objective function $\mathcal{J}(h(f(\mathbf{x})), y)$, and y is the identity corresponding to \mathbf{x} . In the testing phase, \mathbf{x}_e represents the enrolled image corresponding to \mathbf{x} . When the distance $d(f(\mathbf{x}), f(\mathbf{x}_e))$ between the two images is less than a certain threshold, they are judged to be the same subject, otherwise they are different subjects. Note that the fully-connected layer in the supervisory head is no longer needed when the training is finished. Since classification models are limited by the number of categories, it leads to the little discussion of traditional black-box

adversarial attacks on crossing the training set, *i.e.*, the training set between the source model and the black-box model is different. But FRS is not subject to the number of categories, and crossing the training set is a more common case in real-world applications, which is ignored by current researches.

2.2 Adversarial Attack

To obtain the adversarial perturbations δ , we consider ℓ_∞ -norm constrained perturbation in this work, where δ satisfies $\|\delta\|_\infty \leq \epsilon$ with ϵ being the maximum perturbation magnitude. The adversarial black-box attacks can be categorized into two categories: (1) query-based attack needs the feedback of iterative queries to target models, which is not consistent with the assumptions of this paper; (2) Transferability-based attack that use the adversarial examples generated on some surrogate models to attack the other target models. The most common of this type of attacks are gradient-based methods such as FGSM [Goodfellow *et al.*, 2015], MI [Dong *et al.*, 2018], DI [Xie *et al.*, 2019], TI [Dong *et al.*, 2019], SI [Lin *et al.*, 2020], ADMIX [Wang *et al.*, 2021] and some combinations of them. We provide a brief introduction of FGSM to represent this series of methods:

$$\delta = \epsilon \cdot \text{sign}(\nabla_{\mathbf{x}} \mathcal{L}(\mathbf{x}, \mathbf{x}_e; \theta)), \quad (1)$$

where θ is parameter of network, \mathcal{L} is the loss function at the testing phase, usually a negative distance function, and the Euclidean distance is employed as the distance function in this work.

Liu *et al.* [2017b] first proposed to employ ensemble learning in adversarial attack, there is a consensus that the greater the difference in the structure of the ensemble models the better the generated adversarial examples are [Zhang *et al.*, 2021]. Note that our ensemble adversarial attacks integrate identical architecture instead of the typical setting of ensemble adversarial attacks. This sheds light on an alternative way to exploit ensemble learning in adversarial attack. There are also some model-specific designed attacks, *e.g.*, LinBP [Guo *et al.*, 2020] modified the specific activation neurons during the back-propagation, TTP [Naseer *et al.*, 2021] trained a specific generative model, it is non-trivial to extend these findings to other architectures or modules.

2.3 Resisting JPEG Compression

JPEG compression is the most common image compression technique used for image transmission over the web, and is also an adversarial defense [Naseer *et al.*, 2021]. Athalye *et al.* [2018] pointed out that attacker can approximate the non-differentiable JPEG with a differentiable module and regard it as an sub-module of the whole model, and thus derive the gradient-based adversarial perturbation. Shin *et al.* [2018] replaced non-differentiable JPEG with differentiable mathematical functions. Wang *et al.* [2020c] trained a generative network to simulate JPEG and deploy it as an sub-module of the whole model. However, this class of methods can only target JPEG compression of specific factors, *e.g.*, an adversarial example generated for a quality factor of 50 will fail when faced with a JPEG compression with a quality factor of 75. In contrast, other work tried to restrict the perturbation to the low frequency band, which avoids the effect of JPEG

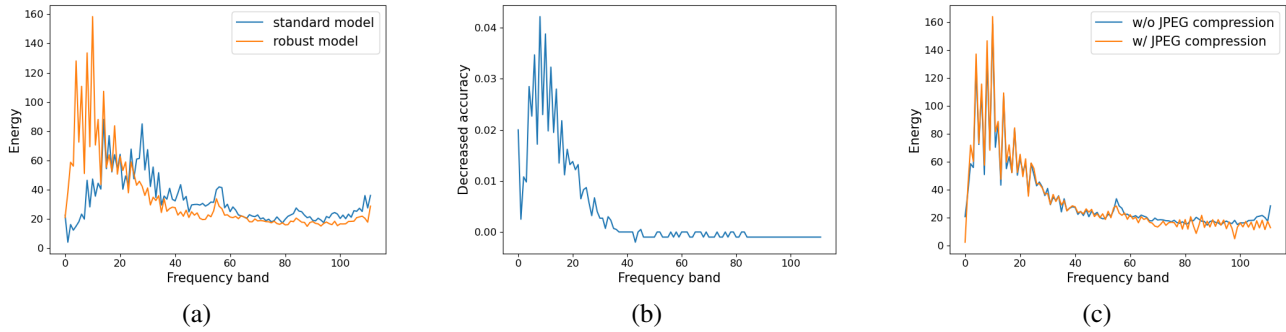


Figure 2: (a) The robust model and standard model utilize different frequency components. (b) Removing different frequency components leads to different decreased accuracy. (c) JPEG compression weakens mainly the high frequency band.

compression. Zhou *et al.* [2018] used a form of low-pass filter to enforce the adversarial perturbation into low frequency band. Yash *et al.* [2019] removed certain high frequency components of the perturbation by the discrete cosine transform (DCT) and inverse discrete cosine transform (IDCT). However, these methods weaken the performance of adversarial perturbation in some cases.

3 Low Frequency Adversarial Perturbation (LFAP)

3.1 Robust Model Utilizing Low Frequency Information

Existing works have shown that the behavior of the model utilizing robust features is highly correlated with the model utilizing low frequency component of images [Wang *et al.*, 2020d; Wang *et al.*, 2020a; Chen *et al.*, 2021]. To justify the feasibility of designing low frequency adversarial perturbation from the source model, we investigate the frequency components contained in the adversarial perturbation. Specifically, we trained a standard model and a robust model on the ILSVRC2012 training dataset, respectively. The robust model was adversarially trained in the radius-4 neighbourhood. We next compared the differences in the frequency domain components of the adversarial perturbations generated by these two models on the validation set. To obtain the frequency domain components of the adversarial perturbations, we compared the energy difference between the original images and the adversarial images in the frequency domain by using DCT. The accumulated energy of the same frequency band is shown in Figure 2(a). We can find that the robust model generates more perturbations in the low frequency band, compared to the standard model. This inspires us to use a robust FRS to generate the adversarial perturbation.

3.2 Methodology

Following the idea of using a robust model to generate low frequency adversarial perturbations, we perform standard adversarial training [Madry *et al.*, 2018] on the FRS:

$$\min_{\theta_f, \theta_H} \mathbb{E}_{(\mathbf{x}, y) \sim D} \left[\max_{\|\delta\|_\infty \leq \epsilon} \mathcal{J}(h(f(\mathbf{x} + \delta)), y; \theta_f, \theta_H) \right], \quad (2)$$

where θ_f and θ_h denote the parameters of the backbone f and the head h , respectively. This allows the model to utilize

information mainly in the low frequency band in the expectation that the adversarial perturbation generated on the robust model contains more low frequency component. Note that once the training of a robust FRS is completed, the head h can be discarded. Therefore, using FGSM as the example, the generation process of *Low Frequency Adversarial Perturbation* (LFAP) only requires substituting the parameters θ in Equation 1 with the parameters θ_f obtained in Equation 2:

$$\delta_{\text{LFAP}} = \epsilon \cdot \text{sign}(\nabla_{\mathbf{x}} \mathcal{L}(\mathbf{x}, \mathbf{x}_e; \theta_f)). \quad (3)$$

The illustration of the generation is shown in Figure 3(a).

4 Low-Mid Frequency Adversarial Perturbation (LMFAP)

4.1 Contribution of Mid Frequency Components

To investigate whether the low frequency perturbation is the best solution, we analyzed the impact of full frequency domain components to FRS. So we transform the images \mathbf{x} to the frequency domain by DCT, then we use a frequency mask to remove the specific frequency domain component, and then reconstruct the image $\mathbf{x}_{\text{masked}}$ from spectrum matrix $\text{DCT}(\mathbf{x})$ by IDCT:

$$\mathbf{x}_{\text{masked}} = \text{IDCT}(\text{DCT}(\mathbf{x}) \cdot M), \quad (4)$$

where M is the mask matrix to remove n -th component, which can be expressed in the following form:

$$M_{i,j} = \begin{cases} 0, & i = n \text{ or } j = n \\ 1, & \text{else} \end{cases}. \quad (5)$$

By testing the decreased accuracy of the reconstructed images $\mathbf{x}_{\text{masked}}$ on the FRS, we can obtain the contribution of the specific frequency component to the FRS. Therefore, we tested the decreased accuracy corresponding to $n \in [1, 112]$, as shown in Figure 2(b). We can find that low frequency band component (about [1, 20] in the LFW dataset) in the image contributes greatly to the model indeed, which also provides an experimental basis for employing low frequency adversarial perturbation in the previous subsection. However the mid frequency band (about [20, 40] in the LFW dataset) component still makes a non-trivial contribution and, as shown in Figure 2(a), the robust model is not proficient in utilizing

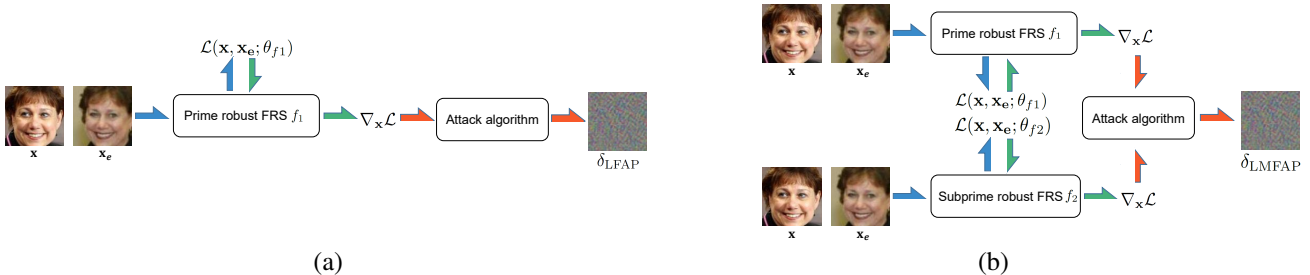


Figure 3: The illustration framework of generating (a) LFAP and (b) LMFAP.

the mid frequency component. This inspires us to integrate these two components to enhance the performance of adversarial perturbation. In addition, we also evaluated the effect of JPEG compression on adversarial perturbation. As shown in the Figure 2(c), we compare the adversarial perturbations with and without JPEG compression, and the result illustrates that JPEG compression weakens mainly the high frequency band (> 50). This also demonstrates the feasibility of using low-mid frequency adversarial perturbations.

4.2 Methodology

As we described in the previous section, the model also utilizes mid frequency component in the image, and this information is also hardly affected by JPEG. In other words, is it possible to design an adversarial perturbation containing part of the mid frequency component as a productive complement to the low frequency component? The key lies in how to integrate the low and mid frequency components in the perturbation. Inspired by employing ensemble learning in adversarial attack [Liu *et al.*, 2017b], we need a model that utilizes relatively low frequency information and another model that utilizes relatively mid frequency information. So we first obtain the prime robust FRS f_1 with θ_{f1} by adversarially training m_1 epochs in the radius- ϵ_1 neighbourhood via Equation (2). Second, still via Equation (2), but we adversarially train m_2 epochs in the radius- ϵ_2 neighborhood to obtain the subprime robust FRS f_2 with θ_{f2} . The values of ϵ_2 and m_2 corresponding to f_2 should be smaller compared to the ϵ_1 and m_1 in order to obtain the model that utilizes relatively mid frequency information. Instead of simply summing the adversarial perturbation generated by the f_1 and f_2 , we use ensemble learning to integrate them. Using FGSM as the example, the generation process of *Low-Mid Frequency Adversarial Perturbation* (LMFAP) can be defined as follows:

$$\delta_{\text{LMFAP}} = \epsilon \cdot \text{sign}(\nabla_x [\mathcal{L}(x, x_e; \theta_{f1}) + \lambda \cdot \mathcal{L}(x, x_e; \theta_{f2})]), \quad (6)$$

where λ is a hyper-parameter that balances the contributions of the two FRSs. The illustration of generation is shown in Figure 3(b).

5 Experiments

5.1 Setups

To extensively evaluate the practical performance of our methods, with the help of the FaceX-Zoo toolbox², we pre-

pared several models with different backbones, supervisory heads, training datasets as test models.

Datasets. We train the source FRS on CASIA-WebFace dataset. The FRSs used to test the adversarial examples (black-box models) are trained on one of three datasets: MS-Celeb-1M (MS) [Guo *et al.*, 2016], CASIA-WebFace (CA) [Yi *et al.*, 2014] and VGGFace2 (VG) [Cao *et al.*, 2018]. LFW, AgeDB-30 and CFP-FP datasets are used as test datasets to verify the effectiveness of the adversarial examples. With the same setup as [Zhang *et al.*, 2020], we aim to jam the unauthorized FRS to match the same users, thus the positive pairs (belong to the same person) are used for testing. In the section, we select subjects with two face images, where one is used as the enrolled image, and the other is the original image for synthesizing the adversarial image.

Models. For backbones, we consider TF-NAS-A, GhostNet, MobileFaceNet (MFNet), Inception-ResNet-v1 (In-Res-v1), ResNet50-ir-se (Res50-i-s), ResNet50-ir (Res50-i), SwinTransformer (SwinT) and Sphere20a. For heads, we consider ArcFace (Arc) [Deng *et al.*, 2019], FaceNet (FN) [Schroff *et al.*, 2015], SphereFace (SF) [Liu *et al.*, 2017a] and MV-Softmax (MV) [Wang *et al.*, 2020b]. Therefore, a FRS can be denoted as backbone@head@training dataset. *E.g.*, the FRS trained on CASIA-WebFace dataset and employing ResNet50-ir backbone and MV-Softmax head can be denoted as ResNet50-i@MV@CA.

Baselines. To show the performance improvement of our methods incorporated with black-box attack algorithms, we employ FGSM, MI, TI, SI, DI-MI, ADMIX and ADMIX-DI-MI as *black-box attack* baselines. To demonstrate the superiority of our methods to resist JPEG compression, we consider Differentiable-jpeg, ComReAdv, TAP and DCT-Low as *resisting JPEG attack* baselines.

Hyper-parameters. For prime robust FRS f_1 , we adopt radius-4 neighborhood adversarial training by SGD optimizer with 0.9 momentum for 50 epochs with the initial learning rate of 0.1 divided by 10 at Epoch 30 and 45, respectively. For subprime robust FRS f_2 , we adopt radius-1 neighborhood adversarial training by SGD optimizer with 0.9 momentum for 20 epochs with the initial learning rate of 0.1 divided by 10 at Epoch 10, respectively, *i.e.*, $\epsilon_1 = 4$, $\epsilon_2 = 1$, $m_1 = 50$, $m_2 = 20$. The maximum perturbation ϵ of each pixel is set to be 8 or 16, the number of iteration is set to be 10, the step size is set to be 1.25. The λ in Equation (6) is set to be 0.6.

²<https://github.com/JDAI-CV/FaceX-Zoo>

Table 1: The black-box attack success rates with the different JPEG compression on LFW dataset. The quality factor of JPEG compression is set to be 75.

Attacks	W/O	Quality=75	Quality=50
Differentiable-JPEG-75	72.30	73.87	70.10
Differentiable-JPEG-50	73.60	73.83	72.2
ComReAdv-75	50.04	48.13	47.57
ComReAdv-50	49.67	47.73	47.53
TAP	74.43	74.20	70.66
DCT-Low	68.00	70.7	67.57
LFAP	77.07	75.66	75.96
LMFAP	96.87	96.26	95.86

5.2 Experimental Results on Resisting JPEG Attacks

Experimental Analysis

To illustrate that restricting the adversarial perturbation to the low frequency band actually weakens its effectiveness, we conduct the experimental analysis between the unconstrained adversarial perturbations (Unconstrained) and the low frequency adversarial perturbations in [Yash *et al.*, 2019] (DCT-Low). Specifically, we used ResNet18, trained on the ILSVRC2012, as the model for generating adversarial perturbations. According to the setup of [Yash *et al.*, 2019], (1) we first generated the adversarial perturbations on all 50,000 validation set images using the FGSM attack, (2) next the high frequency components [180, 224] of the adversarial perturbations were removed by the DCT and IDCT, and (3) finally the attack success rate was tested on the ResNet50. was tested after JPEG compression with a quality factor of 50.

We show the results of DCT-Low and the unconstrained perturbations in different scenarios as shown in the Figure 1. We can find that, (1) the attack success rate of Unconstrained (w/ JPEG on black-box) is lower than Unconstrained (w/o JPEG on black-box). The decreased rate proves that JPEG compression weakens the effectiveness of adversarial perturbation; (2) The attack success rate of DCT-Low (w/ JPEG on black-box) is higher than Unconstrained (w/ JPEG on black-box). This indicates that this low frequency adversarial perturbation has more capability to resist JPEG compression compared to the original perturbation. However, (3) without JPEG compression, the attack success rate of DCT-Low (w/o JPEG on black-box) is lower than Unconstrained (w/o JPEG on black-box). Moreover, (4) in the real-world application scenario, *i.e.*, the generated adversarial images need to be processed by JPEG compression and tested on black-box models, DCT-Low (w/ JPEG on black-box) performs better the Unconstrained (w/ JPEG on black-box). But in the interference-free scenario, DCT-Low (w/o JPEG on white-box) performs worse the Unconstrained (w/o JPEG on white-box). The two finding illustrates that restricting the adversarial perturbation weaken the performance of adversarial perturbation in some cases. So a more natural way is to reconstruct the source model to use low frequency information, and then use this model to generate the low frequency adversarial perturbation.

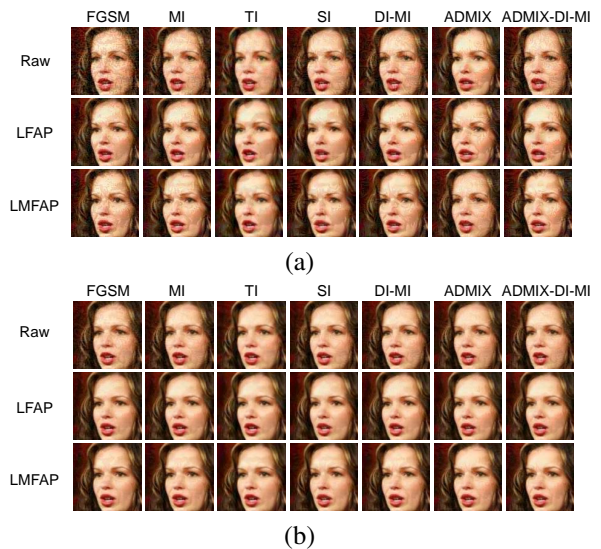


Figure 4: The example adversarial images. Seven columns correspond to seven different baseline attacks, the first row corresponds to the raw baseline attack, and the second and third rows represent the attacks Incorporated with LFAP and LMFAP, respectively. (a) The ϵ is set to be 16. (b) The ϵ is set to be 8.

Comparison with Resisting JPEG Attacks

To demonstrate the performance improvement of our methods compared to existing methods that resist JPEG compression, we compare our method with 4 baseline attacks on MFNet@MV@CA under the $\epsilon = 16$, the results of generated adversarial images after the JPEG compression with different quality factors are shown in Table 1. It should be noted that in order to get fair comparison results, the adversarial attack algorithm we employed in Table 1 to generate adversarial examples is ADMIX-DI-MI. The experimental results on different datasets and different ϵ are shown in the supplementary material. We can observe that: (1) The method tackling target JPEG compression of specific factors underperform when faced with other factors. *E.g.*, Differentiable-JPEG-75 achieves worse performance without JPEG compression than when the compression quality factor= 75. (2) Our method (LMFAP) achieves the best performance on all situations. (3) The stronger performance of LMFAP over LFAP indicates that our incorporation strategy is effective for different compression qualities.

5.3 Experimental Results on Black-box Attacks

To demonstrate that our methods can be incorporated with existing black-box attacks and improve their performance, we evaluated 7 baseline attacks and incorporated attacks on 9 FRSs under the $\epsilon = 16$, and the results of generated adversarial images on LFW dataset are shown in Table 2. We show the examples of generated adversarial images in Figure 4. The experimental results on different datasets and different ϵ are shown in the supplementary material. We have the following main findings: (1) Our method, LMFAP incorporated with ADMIX-DI-MI, *i.e.*, the state-of-the-art black-box attack, achieves the best performance than all

Table 2: The black-box attack success rates on LFW dataset.

Attacks	TF-NAS-A@MV@MS	GhostNet@MV@MS	SwinT@MV@MS	MFNet@MV@MS	MFNet@MV@CA	MFNet@Arc@CA	In-Res-vl@FN@VG	ResNet50-i-s@Arc@MS	Sphere20a@SF@CA
FGSM	29.05	29.36	15.61	31.80	72.66	44.38	33.30	27.68	62.05
FGSM-LFAP	39.51	33.96	29.84	33.59	58.33	48.98	48.36	35.88	47.11
FGSM-LMFAP	64.15	59.76	49.71	59.63	83.63	73.01	64.56	62.28	66.11
MI	16.21	16.30	6.61	16.33	48.26	27.98	15.33	15.41	32.65
MI-LFAP	51.08	46.16	40.35	44.26	71.09	62.61	55.13	47.58	56.68
MI-LMFAP	83.41	79.16	71.55	78.83	93.46	89.68	77.59	82.78	81.08
TI	7.28	7.16	3.15	7.56	37.36	12.18	17.43	7.48	19.08
TI-LFAP	15.15	16.16	8.11	13.30	41.20	21.41	42.73	14.98	27.78
TI-LMFAP	43.61	42.30	26.91	37.86	78.23	53.25	67.63	44.78	53.85
SI	22.55	24.16	11.55	27.63	53.90	38.78	30.46	22.05	55.05
SI-LFAP	48.08	43.53	36.05	41.66	67.19	60.11	52.26	44.28	54.65
SI-LMFAP	83.18	78.93	69.81	77.90	92.79	89.41	75.36	81.71	79.78
DI-MI	22.61	22.43	9.44	22.73	57.43	34.71	21.46	22.91	40.88
DI-MI-LFAP	53.48	48.49	41.61	45.99	72.36	64.68	59.20	49.34	59.54
DI-MI-LMFAP	86.01	82.03	75.05	81.03	94.53	91.45	81.23	85.58	84.08
ADMIX	15.08	16.76	5.68	18.43	52.16	29.41	14.49	16.68	31.25
ADMIX-LFAP	53.21	47.90	39.65	45.53	73.46	64.51	54.46	46.81	58.71
ADMIX-LMFAP	88.11	85.46	77.75	84.50	95.89	93.51	81.23	88.11	86.81
ADMIX-DI-MI	33.28	32.36	16.65	34.43	71.90	49.55	29.16	33.18	47.45
ADMIX-DI-MI-LFAP	59.08	52.79	46.28	49.96	75.76	68.08	63.16	53.68	61.84
ADMIX-DI-MI-LMFAP	89.35	87.33	79.54	86.20	96.19	94.08	84.96	90.31	88.01

existing black-box attacks. The attack success rates are almost always above 80.0%, especially a margin of 39.74% than the state-of-the-art ADMIX-DI-MI on average. This demonstrates the performance of our methods in resisting JPEG compression and facing unknown FRSs. (2) Our methods (both LFAP and LMFAP) are compatible with various black-box attacks. Almost all black-box attacks can significantly improve performance when incorporated with our methods (both LFAP and LMFAP). The stronger the black-box attack, the better performance the incorporated attack achieves. This suggests us to use more effective black-box attack when deploying the incorporated framework in practical applications. (3) LMFAP basically outperforms LFAP, which proves that our incorporation strategy is effective. (4) By comparing MFNet@MV@MS, MFNet@MV@CA and MFNet@Arc@CA, rather than the different backbones, we find that the other different black-box settings in the FRS also have an effect on the black-box attacks, *i.e.*, the training set and the head. This is an undiscussed finding for researchers studying black-box attacks in FRSs.

6 Conclusion

In this paper, we investigated how adversarial perturbations achieve better performance of resisting JPEG compression. We first analyzed the limitations of the existing method for generating low frequency perturbation, and employ robust training process to design the LFAP. Second, by analyzing the contribution of the full frequency domain component to the model, we presented the refined LMFAP, which is the adversarial perturbation containing part of the mid frequency component as a productive complement. Third, experiments on several settings demonstrate that our methods outperform the resisting JPEG compression methods and existing black-box methods.

References

[Athalye *et al.*, 2018] Anish Athalye, Nicholas Carlini, and David Wagner. Obfuscated gradients give a false sense of security: Circumventing defenses to adversarial examples. In *ICML*, pages 274–283, 2018.

[Cao *et al.*, 2018] Qiong Cao, Li Shen, Weidi Xie, Omkar M Parkhi, and Andrew Zisserman. Vggface2: A dataset for recognising faces across pose and age. In *FG*, pages 67–74, 2018.

[Chen *et al.*, 2021] Guangyao Chen, Peixi Peng, Li Ma, Jia Li, Lin Du, and Yonghong Tian. Amplitude-phase recombination: Rethinking robustness of convolutional neural networks in frequency domain. In *ICCV*, pages 458–467, 2021.

[Deng *et al.*, 2019] Jiankang Deng, Jia Guo, Niannan Xue, and Stefanos Zafeiriou. Arcface: Additive angular margin loss for deep face recognition. In *CVPR*, pages 4690–4699, 2019.

[Dong *et al.*, 2018] Yinpeng Dong, Fangzhou Liao, Tianyu Pang, Hang Su, Jun Zhu, Xiaolin Hu, and Jianguo Li. Boosting adversarial attacks with momentum. In *CVPR*, pages 9185–9193, 2018.

[Dong *et al.*, 2019] Yinpeng Dong, Tianyu Pang, Hang Su, and Jun Zhu. Evading defenses to transferable adversarial examples by translation-invariant attacks. In *CVPR*, pages 4312–4321, 2019.

[Goodfellow *et al.*, 2015] Ian J Goodfellow, Jonathon Shlens, and Christian Szegedy. Explaining and harnessing adversarial examples. *ICLR*, 2015.

[Guo *et al.*, 2016] Yandong Guo, Lei Zhang, Yuxiao Hu, Xiaodong He, and Jianfeng Gao. Ms-celeb-1m: A dataset and benchmark for large-scale face recognition. In *ECCV*, pages 87–102, 2016.

[Guo *et al.*, 2020] Yiwen Guo, Qizhang Li, and Hao Chen. Backpropagating linearly improves transferability of adversarial examples. *NeurIPS*, 2020.

[Lin *et al.*, 2020] Jiadong Lin, Chuanbiao Song, Kun He, Liwei Wang, and John E Hopcroft. Nesterov accelerated gradient and scale invariance for adversarial attacks. In *ICLR*, 2020.

[Liu *et al.*, 2017a] Weiyang Liu, Yandong Wen, Zhiding Yu, Ming Li, Bhiksha Raj, and Le Song. Sphereface: Deep hypersphere embedding for face recognition. In *CVPR*, pages 212–220, 2017.

[Liu *et al.*, 2017b] Yanpei Liu, Xinyun Chen, Chang Liu, and Dawn Song. Delving into transferable adversarial examples and black-box attacks. *ICLR*, 2017.

[Madry *et al.*, 2018] Aleksander Madry, Aleksandar Makelov, Ludwig Schmidt, Dimitris Tsipras, and Adrian Vladu. Towards deep learning models resistant to adversarial attacks. In *ICLR*, 2018.

[Naseer *et al.*, 2021] Muzammal Naseer, Salman Khan, Munawar Hayat, Fahad Shahbaz Khan, and Fatih Porikli. On generating transferable targeted perturbations. *arXiv preprint arXiv:2103.14641*, 2021.

[Schroff *et al.*, 2015] Florian Schroff, Dmitry Kalenichenko, and James Philbin. Facenet: A unified embedding for face recognition and clustering. In *CVPR*, pages 815–823, 2015.

[Shin and Song, 2018] Richard Shin and Dawn Song. Jpeg-resistant adversarial images. In *NIPS 2017*, 2018.

[Wang *et al.*, 2020a] Haohan Wang, Xindi Wu, Zeyi Huang, and Eric P Xing. High-frequency component helps explain the generalization of convolutional neural networks. In *CVPR*, pages 8684–8694, 2020.

[Wang *et al.*, 2020b] Xiaobo Wang, Shifeng Zhang, Shuo Wang, Tianyu Fu, Hailin Shi, and Tao Mei. Mis-classified vector guided softmax loss for face recognition. In *AAAI*, pages 12241–12248, 2020.

[Wang *et al.*, 2020c] Zhibo Wang, Hengchang Guo, Zhifei Zhang, Mengkai Song, Siyan Zheng, Qian Wang, and Ben Niu. Towards compression-resistant privacy-preserving photo sharing on social networks. In *ACM MobiHoc*, pages 81–90, 2020.

[Wang *et al.*, 2020d] Zifan Wang, Yilin Yang, Ankit Shrivastava, Varun Rawal, and Zihao Ding. Towards frequency-based explanation for robust cnn. *arXiv preprint arXiv:2005.03141*, 2020.

[Wang *et al.*, 2021] Xiaosen Wang, Xuanran He, Jingdong Wang, and Kun He. Admix: Enhancing the transferability of adversarial attacks. *arXiv preprint arXiv:2102.00436*, 2021.

[Xie *et al.*, 2019] Cihang Xie, Zhishuai Zhang, Yuyin Zhou, Song Bai, Jianyu Wang, Zhou Ren, and Alan L Yuille. Improving transferability of adversarial examples with input diversity. In *CVPR*, pages 2730–2739, 2019.

[Yash *et al.*, 2019] Sharma Yash, Ding Gavin Weiguang, and A. Brubaker Marcus. On the effectiveness of low frequency perturbations. In *IJCAI*, pages 3389–3396, 2019.

[Yi *et al.*, 2014] Dong Yi, Zhen Lei, Shengcai Liao, and Stan Z Li. Learning face representation from scratch. *arXiv preprint arXiv:1411.7923*, 2014.

[Zhang *et al.*, 2020] Jiaming Zhang, Jitao Sang, Xian Zhao, Xiaowen Huang, Yanfeng Sun, and Yongli Hu. Adversarial privacy-preserving filter. In *ACM MM*, pages 1423–1431, 2020.

[Zhang *et al.*, 2021] Jiaming Zhang, Jitao Sang, Kaiyuan Xu, Shangxi Wu, Xian Zhao, Yanfeng Sun, Yongli Hu, and Jian Yu. Robust captchas towards malicious ocr. *IEEE Transactions on Multimedia*, 23:2575–2587, 2021.

[Zhou *et al.*, 2018] Wen Zhou, Xin Hou, Yongjun Chen, Mengyun Tang, Xiangqi Huang, Xiang Gan, and Yong Yang. Transferable adversarial perturbations. In *ECCV*, pages 452–467, 2018.